



# Tracking the invasion of breast cancer cells in paper-based 3D cultures by OCT motility analysis

JULIE C. MCINTOSH,<sup>1,6</sup> LIN YANG,<sup>2,6</sup> TING WANG,<sup>3</sup> HAIBO ZHOU,<sup>3</sup>  
MATTHEW R. LOCKETT,<sup>1,4</sup>  AND AMY L. OLDENBURG<sup>2,4,5,\*</sup>

<sup>1</sup>Department of Chemistry, University of North Carolina-Chapel Hill, Chapel Hill, NC 27599, USA

<sup>2</sup>Department of Physics and Astronomy, University of North Carolina-Chapel Hill, Chapel Hill, NC 27599, USA

<sup>3</sup>Department of Biostatistics, University of North Carolina-Chapel Hill, Chapel Hill, NC 27599, USA

<sup>4</sup>Lineberger Comprehensive Cancer Center, University of North Carolina-Chapel Hill, Chapel Hill, NC 27599, USA

<sup>5</sup>Biomedical Research Imaging Center, University of North Carolina-Chapel Hill, Chapel Hill, NC 27599, USA

<sup>6</sup>Co-first authors contributed equally and are listed alphabetically

\*aold@physics.unc.edu

**Abstract:** 3D paper-based cultures (PBCs) are easy-to-use and provide a biologically representative microenvironment. By stacking a sheet of cell-laden paper below sheets containing cell-free hydrogel, we form an assay capable of segmenting cells by the distance they invaded from the original cell-seeded layer. These invasion assays are limited to end-point analyses with fluorescence-based readouts due to the highly scattering nature of the paper scaffolds. Here we demonstrate that optical coherence tomography (OCT) can distinguish living cells from the surrounding extracellular matrix (ECM) or paper fibers based upon their intracellular motility amplitude ( $M$ ).  $M$  is computed from fluctuation statistics of the sample, rejects shot noise, and is invariant to OCT signal attenuation. Using OCT motility analysis, we tracked the invasion of breast cancer cells over a 3-day period in 4-layer PBCs (160–300  $\mu\text{m}$  thick) *in situ*. The cell population distributions determined with OCT are highly correlated with those obtained by fluorescence imaging, with an intraclass correlation coefficient (ICC) of 0.903. The ability of OCT motility analysis to visualize live cells and quantify cell distributions in PBC assays *in situ* and longitudinally provides a novel means for understanding how chemical gradients within the tumor microenvironment affect cellular invasion.

© 2020 Optical Society of America under the terms of the [OSA Open Access Publishing Agreement](#)

## 1. Introduction

Cellular invasion, a process in which cells remodel their surrounding extracellular matrix (ECM) prior to moving into neighboring tissue, plays an important role in tissue formation and maintenance as well as in disease progression. In carcinomas, invasion of cancerous cells through the basement membrane is the first step towards metastasis, which is a leading cause of cancer-related deaths in the US [1]. Traditionally, movement is investigated with migration assays, which quantify cellular movement along a two-dimensional (2D) surface or across a porous membrane. Three-dimensional (3D) cultures are a more representative model system for studying invasion because the cells must sever cell-cell contacts and degrade the surrounding ECM before movement [2–5]. The paper-based culture (PBC) platform we developed provides several experimental advantages over other 3D invasion assays [6–9], including the ability to easily segment populations of cells based on the distance invaded without the need for fixation or histological slicing [10,11].

Paper-based invasion assays are comprised of several sheets of paper stacked together, where cells from a single cell-containing sheet invade into neighboring cell-free sheets. The modularity of the stacking method allows for tissue-like structures to be assembled by incorporating different numbers of either a cell-laden or cell-free paper sheets [10–13]. We and others have quantified the invasion of both carcinoma and stromal cells in PBCs containing either mono- or co-cultures [10–12,14,15]. With these invasion assays, we showed cells placed in diffusion-limited environments containing monotonic gradients of oxygen, nutrients, and waste products invade regions of higher oxygen tension preferentially [10,12].

To quantify cellular movement in these assays, we relied on confocal fluorescence imaging and microscopy [12,16,17]. The opaque and highly scattering nature of the cellulose fibers in the paper scaffolds limits the imaging depth, requiring the culture to be disassembled prior to analysis. End-point analyses increase biological and technical variability within a dataset as a separate culture must be prepared for each time point. The ability to repeatedly analyze a single culture *in situ*, without damaging the cells, would enable longitudinal studies as well as increase the experimental information density while minimizing sample-to-sample variation.

Here, we propose an optical coherence tomography (OCT)-based method to address the limitations of confocal fluorescence imaging in multilayer PBCs. OCT is a biomedical imaging modality based upon low-coherence interferometry that provides non-invasive, micron-resolution, depth-resolved images by sensing near-infrared light backscattered from tissue [18]. While OCT is widely used in clinical imaging, it is increasingly being explored for microscopy applications where light scattering limits the imaging depth. OCT offers superior depth-resolution to conventional microscopy by rejecting multiply-scattered photons outside the coherence gate, enabling imaging over several scattering mean free paths into biological tissue [19]. Previous studies have demonstrated the utility of OCT for imaging optically thick, 3D cultures such as organoids and spheroids *in situ*, longitudinally, and label-free [20,21]. OCT has also been used to track cellular movement in both 2D and 3D culture formats [22–24].

Dynamic OCT signals (*i.e.*, speckle fluctuations) provide additional information such as the ability to contrast live cells against light scattering background materials [25]. Intracellular dynamics, such as organelle transport and membrane undulations, give rise to OCT speckle fluctuations with characteristic frequencies of  $\sim 10$  mHz – 10 Hz [26]. These cellular motions occur on a sub-wavelength (nanometer) scale with typical speeds of 5–2000 nm/s [27]. Speckle fluctuation signals have thus been shown to differentiate viable cells from non-viable cells and background materials [25,28–30]. A particularly useful, quantitative metric derived from OCT speckle fluctuations is an autocorrelation-based standard deviation known as the motility amplitude ( $M$ ) [31]. This metric is unique in that it omits shot noise and is invariant with respect to image depth and signal-to-noise ratio (SNR). These features are crucial for controlling against the strong depth-dependent signal attenuation in OCT, and day-to-day variations in OCT system sensitivity, thus enabling comparison of  $M$  across multiple locations in the sample and across experiments. Previously, we found that  $M$  was a sensitive indicator of cell-cell interactions, toxicant exposures and motility suppression mechanisms [28,31–32]. We also showed that  $M$  highly correlates to cell viability, as measured with a standard MTT assay [28].

In this study, we used  $M$  to identify live cells in PBCs and subsequently track their movement throughout an invasion stack. All experiments were performed with MDA-MB-231 cells, a highly invasive, triple-negative breast cancer line with a well-characterized mesenchymal phenotype [33]. Initially, we showed that the signals generated by traditional fluorescence imaging correlate to  $M$ , enabling  $M$  to be used as a viability metric. Next, we determined that the cell distribution from the same end-point invasion assay were equivalent for both imaging techniques. Finally, we showed that OCT was able to track cellular invasion with longitudinal measurements without disturbing the cell population. Compared to previous work on cell invasion, this paper constitutes the first study to successfully track live cells in 3D within a highly light scattering background material

(paper) over greater depth than accessible by confocal fluorescence imaging, in a non-invasive, and label-free manner. Furthermore, our study demonstrates OCT-based measurements can longitudinally track invasion over longer time scales (several days) than previous studies (several hours). All of these new capabilities are enabled by the use of the depth-invariant, live cell-specific metric  $M$  in OCT.

## 2. Methods

### 2.1. Cell culture

MDA-MB-231 cells were obtained from the American Type Culture Collection (ATCC) and engineered to constitutively express mCherry fluorescent protein with LPP-MCHR-Lv105-025 lentiviral particles (GeneCopoeia), following the manufacturer's protocol. Cells were maintained as adherent cultures at 37 °C and 5% CO<sub>2</sub> in RPMI medium supplemented with 25 mM HEPES, 10% fetal bovine serum (FBS), and 1% PenStrep. Cell culture medium and supplements were purchased from Gibco except for FBS (VWR). The medium was exchanged every 48 hours, and cells passed at 80% confluency with TrypLE, using standard procedures.

### 2.2. Paper-based cellular invasion assays

The preparation and sterilization of the wax-patterned paper scaffolds was detailed previously [12,13,16]. Each 40 μm-thick scaffold was a wax-patterned sheet of Whatman 105 paper. Each scaffold contained nine independent, wax-free regions that were 2.85 mm in diameter. We refer to these wax-free regions as zones. For every experiment, the zones were seeded with 0.5 μL of either cell-free or cell-laden Matrigel, where Matrigel is a biomimetic ECM. The cell-laden zones contained 80,000 cells ( $3.1 \times 10^8$  cells/cm<sup>3</sup>). Following seeding, the scaffolds were incubated in culture medium at 37°C and 5% CO<sub>2</sub> for 4 hours before assembly.

Figure 1(b) is a schematic of an invasion culture, which is comprised of a single cell-laden scaffold placed below three cell-free scaffolds. When in this stack configuration, each scaffold is considered a layer. The cell-laden layer was designated 0. The cell-free layers were designated +1, +2, and +3 to indicate their position relative to the cell-laden layer. Within a stack, the zones align as nine columns. Each of these columns supports an invasion assay, forming an array of nine technical replicates per stack. The assembled stack was sandwiched between a pair of polyethylene terephthalate (PET) films and then placed in a stainless-steel holder. The PET films limited exchange with the medium to the top of the stack. The holder ensured the layers were in conformal contact throughout the experiment. The presence of the hydrogel in each layer and the compression caused by the holder resulted in the assay center to be 250–300 μm thick, while the edges were around 160 μm. When fully assembled, we refer to this setup as a culture. Each assembled culture was maintained in 6 mL of culture medium within a 6-well plate (Corning). Cell-free cultures were also prepared for each experiment. These cultures contained four layers, where all nine zones were seeded with cell-free Matrigel. The cell-free cultures were used to determine the background signals for fluorescence imaging and the threshold value of  $M$  for OCT. For each experiment, all cultures were prepared from a single passage of cells on Day 0.

### 2.3. Fluorescence imaging and analysis

Prior to fluorescence imaging, the invasion cultures were de-stacked, and each scaffold washed with 1X phosphate buffered saline. Images were acquired on a Typhoon 9400 confocal fluorescence scanner at a 200 μm resolution with a 532 nm laser and a 610BP30 filter. Images were analyzed with FIJI (NIH) [34]. The area-averaged fluorescence intensity,  $I_{Li}$ , of each zone in each layer (layer index  $Li = 0 \dots 3$ ) was determined as follows: (1) The limit of detection (LOD) was determined with Eq. (1), where the background intensity,  $\bar{I}_{bg}$ , is the average intensity of all zones within every layer (36 total zones) of a cell-free culture and  $S_{bg}$  is their standard deviation.

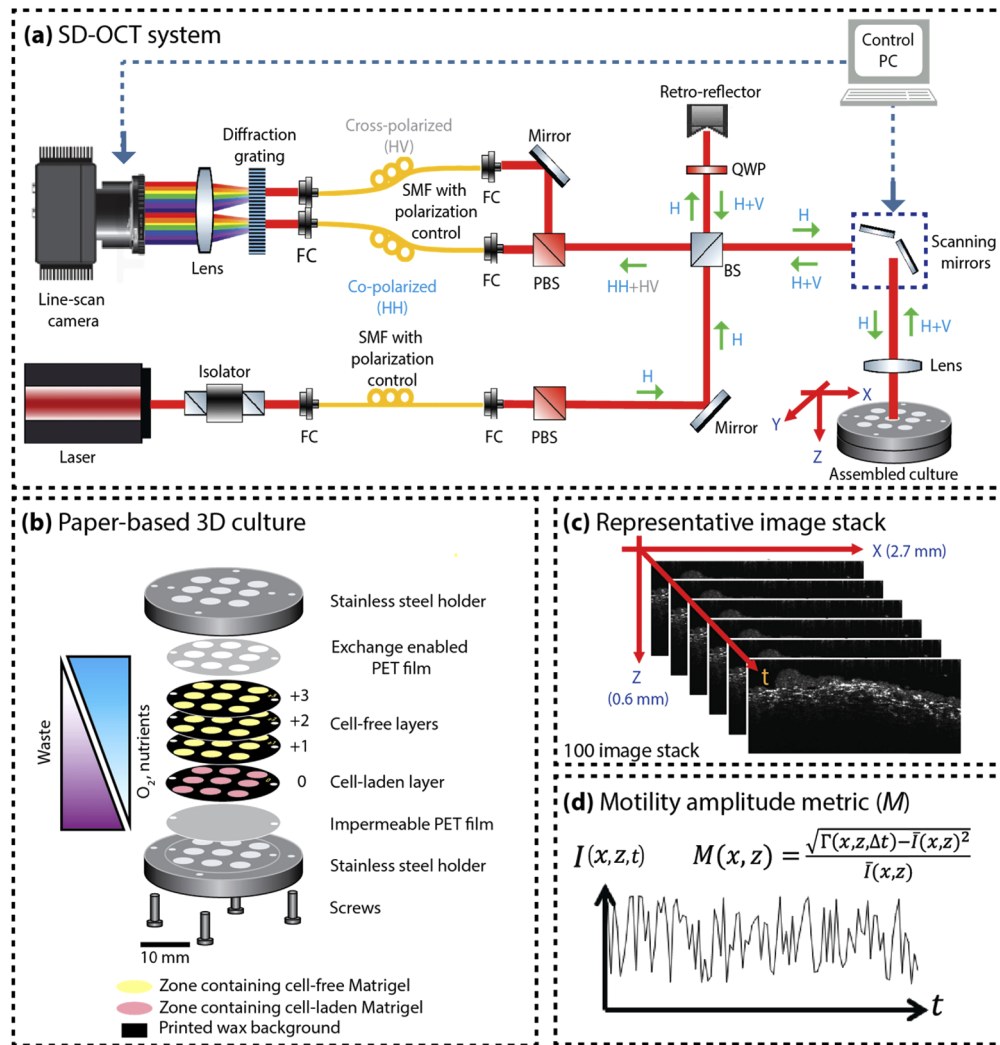


**Fig. 1.** (a) Schematic of the spectral-domain optical coherence tomography (SD-OCT) system: FC, fiber coupler; BS, beam splitter; PBS, polarized beam splitter; QWP, quarter-wave plate at  $22.5^\circ$ ; and SMF, single-mode fiber. (b) Schematic of the PBC invasion culture. (c) Representative time-lapse OCT of a PBC collected as a stack of B-mode (lateral ( $x$ ) by axial ( $z$ )) images in time ( $t$ ). (d) Spatially-resolved motility amplitude metric,  $M(x, z)$ , defined by  $I(x, z, t)$ , the OCT image intensity;  $\bar{I}(x, z)$ , the time average of image intensity over the stack, and  $\Gamma(x, z, \Delta t)$ , the autocorrelation of  $I(x, z, t)$  computed at the B-mode frame sampling time  $\Delta t$ .

A cell-free culture was imaged simultaneously with every cell-laden culture. We chose this definition of LOD because it is commonly used in spectrophotometric methods [35]. (2) The background-subtracted intensity,  $BSI_{Li}$ , was calculated by  $(I_{Li} - \bar{I}_{bg})$ . (3) The percent population per layer,  $P_{Li}$ , was then computed according to Eqn. (2), where, if  $I_{Li}$  was less than the LOD, we set the corresponding  $P_{Li}$  value to 0.

$$LOD = \overline{I_{bg}} + 3S_{bg} \quad (1)$$

$$P_{Li} = \left\{ \begin{array}{ll} \frac{BSI_{Li}}{\sum_{L=0}^3 BSI_{Li}}, & I_{Li} \geq LOD \\ 0, & I_{Li} < LOD \end{array} \right\} \quad (2)$$

## 2.4. OCT imaging and motility analysis

### 2.4.1. Experimental setup and data acquisition

Imaging was performed using the customized, spectral-domain OCT system shown in Fig. 1(a) and detailed previously [36]. Briefly, the light source was a broadband (120 nm) Ti:Sapphire laser (KMLabs, Inc.) centered at 800 nm. Linearly polarized (H-polarized) sample arm light (~6 mW) was focused onto the sample. The backscattered light subsequently interfered with the reference arm light, where spectral interferograms of the co-polarized (HH) components were sampled by the first 2048 pixels of a line scan CCD camera (Basler Sprint) at an A-line rate of 25 kHz. The resolution of the OCT system was ~ 10  $\mu\text{m}$   $\times$  3.0  $\mu\text{m}$  (in aqueous medium) in  $x \times z$ , and the SNR was ~ 108 dB. B-mode (cross-sectional) image frames of 1000  $\times$  1024 pixels were collected over 3  $\times$  1.55 mm (in aqueous medium) in  $x \times z$ , respectively. Time stacks comprised of 100 repetitive B-mode image frames were collected at a frame rate of  $4 \pm 0.004$  Hz at specific lateral locations in  $y$ . This temporal sampling was chosen to capture the frequency spectrum of cellular dynamics [28,31]. Time stacks were collected at 21–31 sampling locations over  $y$ , with a step size of 100  $\mu\text{m}$ , to cover each zone. Four of the nine seeded zones of each invasion culture were imaged in this way.

### 2.4.2. Image analysis

Image rendering and analysis was performed as described previously [21,28,31]. Briefly, B-mode OCT images were computed from raw spectral interferograms after reference subtraction and digital dispersion compensation [37]. The intensity at each pixel,  $I(x, z)$ , was computed from the absolute value of the Fourier transformed spectral-domain OCT signal. Figure 1(c) is a representative stack of time-lapse OCT images, while Fig. 1(d) shows an example of the temporal fluctuations of intensity,  $I(x, z, t)$ , obtained from a time stack. Subsequent motility analysis was performed using Eqn. (3) to quantify  $I(x, z, t)$  with the “motility amplitude” metric  $M(x, z)$ , which is an autocorrelation-based modified standard deviation that is normalized by average pixel intensity [28,31].

$$M(x, z) = \frac{\sqrt{\Gamma(x, z, \Delta t) - \bar{I}(x, z)^2}}{\bar{I}(x, z)} \quad (3)$$

Here,  $\Gamma(x, z, \Delta t)$  is the autocorrelation at each image pixel computed at a frame sampling time of  $\Delta t = 0.25$  s and  $\bar{I}(x, z)$  is the average of  $I(x, z, t)$  over 25 s.  $M$  provides two complementary benefits for data analysis: (1) the autocorrelation at each image pixel,  $\Gamma(x, z, \Delta t)$ , naturally omits shot noise that decorrelates instantaneously while capturing cellular fluctuations (*e.g.*, organelle transport and membrane undulations) that decorrelate on a longer time scale (from  $2\Delta t = 0.5$  s up to the 25 s total time of the measurement), and (2) normalization by average pixel intensity eliminates the depth-dependent SNR roll-off, making the motility amplitude both signal- and

depth-invariant. Ultimately, in each time stack,  $I(x, z, t)$  was analyzed to produce a motility image  $M(x, z)$ , and the  $M(x, z)$  produced from each sampled location in  $y$  across the zone was assembled into a 3D set of data  $M(x, y, z)$  for each zone.

To eliminate signals from stationary background materials (*e.g.*, cell scaffolds and dead cells), we empirically determined a threshold value for  $M$  using the following steps: (1) A region of interest (ROI) was determined manually through visual identification of the four-layer stack within each time-averaged image collected from a cell-free invasion assay. (2)  $M(x, z)$  values within the ROI of each corresponding motility image were extracted and compiled into an array. (3) An average and standard deviation of  $M$  were used to calculate the LOD, similar to that defined in Eq. (1), where the average of  $M$  is  $\bar{I}_{bg}$  and the standard deviation is  $S_{bg}$ . Finally, LODs obtained for all cell-free images within each of 15 assays ( $n = 44$  total ROIs analyzed) collected from four independent experiments were averaged to determine a final threshold of 0.27. This threshold was applied in all subsequent OCT analyses.

For tracking cell invasion, further segmentation of  $M(x, y, z)$  data into regions corresponding to each paper layer was applied. For ease of comparison between the two techniques, which quantify different cellular phenomena (*i.e.*, fluorescent protein expression vs. intracellular motility), we report the OCT results as  $P_{Li}$ , as defined for fluorescence imaging analysis. The following steps were used to calculate  $P_{Li}$  with Eq. (4): (1) Each time-averaged OCT image at a  $y$  position,  $\bar{I}(x, z)$ , was manually segmented into four ROIs, each representing a layer,  $Li$ , within the invasion assay. The manual segmentation was performed by visual identification of the apparent gaps between paper layers in the time-averaged image only, to mitigate bias about the cell distribution. (2) The previously determined threshold value,  $M_{th} = 0.27$ , was applied to  $M$  to reject background noise. (3) The number of pixels,  $N_{Li}$ , with  $M > M_{th}$  were counted for each  $Li$  at each  $y$  position and then accumulated over frames in  $y$  across the zone. (4) The  $N_{Li}$  were then normalized into  $P_{Li}$ , according to the following equation:

$$P_{Li} = \frac{N_{Li}(M > M_{th})}{\sum_0^3 N_{Li}(M > M_{th})} \times 100 \quad (4)$$

## 2.5. Statistics

### 2.5.1. Comparison of imaging methods

An intraclass correlation coefficient (ICC) was used to determine if the  $P_{Li}$  values generated by OCT and from fluorescence images were similar. An ICC, which quantifies the likelihood that observations within the same cluster are more homogeneous than the observations in different clusters, was chosen over the more commonly used Pearson Coefficient calculation because the  $P_{Li}$  values obtained from a single stack are dependent upon one another [38,39].

### 2.5.2. Comparison of cellular distributions in the invasion stacks

To determine if the overall cell distributions between invasion cultures were equivalent, we tested multiple equivalent hypotheses,  $H_{i0} : \mu_{1i} = \mu_{2i}$  vs.  $H_{ia} : \mu_{1i} \neq \mu_{2i}$ . Here,  $\mu_{ki}$  is the mean population percentage of the  $i$ th layer (0, 1, 2 or 3) for each  $k$ th group (OCT or fluorescence images). A simple pairwise comparison of  $P_{Li}$  is not appropriate for this comparison due to the dependency between layers and the requirement that the sum of  $P_{Li}$  is 100%. Instead, we employed the Holm-Bonferroni test procedure on orthogonally transformed variables [40]. This testing procedure is sequentially rejective for multiple comparisons of different layers between two groups and controls for the overall Type I error (false positive) rate for all comparisons. First, we made an orthogonal transformation to the data using Eq. (5), reducing the original vector from 4 to 3. This orthogonal transformation changes the data vector from four constrained percentage variables to a vector of three orthogonal variables that places emphasis on different

layers in the original data. This reduction resulted in a new set of multiple equivalent hypotheses:  $H_{i0} : \bar{\mu}_{1i} = \bar{\mu}_{2i}$  vs.  $H_{ia} : \bar{\mu}_{1i} \neq \bar{\mu}_{2i}$ . Here  $\bar{\mu}_{ki}$  is the mean of the transformed variable of the  $i$ th layer in the  $k$ th group.

$$\begin{pmatrix} V_1 \\ V_2 \\ V_3 \end{pmatrix} = \begin{bmatrix} -3 & -1 & 1 & 3 \\ 1 & -1 & -1 & 1 \\ -1 & 3 & -3 & 1 \end{bmatrix} \begin{pmatrix} P_{L0} \\ P_{L1} \\ P_{L2} \\ P_{L3} \end{pmatrix} \quad (5)$$

Next, we tested the univariate normality of each orthogonal variable with a Shapiro-Wilk test. If all vector elements were from a normal distribution, then each of the three orthogonal transformed variables between the two groups were compared with a paired  $t$ -test. If all vector elements were not from a normal distribution, then the three orthogonal transformed variables between the two groups were compared with a Wilcoxon rank sum test. Finally, we used the Holm-Bonferroni test procedure to adjust the  $p$ -values for each variable. Adjusted  $p$ -values above the pre-specified significance level of 0.05 accepted the null hypothesis and the cell distributions of two groups were statistically equivalent.

### 3. Results and discussion

#### 3.1. OCT motility analysis differentiates zones with and without cells

To demonstrate that  $M$  enables one to distinguish live cells from the paper fibers and background ECM, we performed OCT motility analysis on cell-laden and cell-free cultures, that had both been incubated for 3 days prior to analysis, where the OCT operator was blinded to the identities of the cultures. Figures 2(a) and (b) are representative motility-contrasted OCT images of a cell-laden and cell-free culture, respectively. The blue image is the time-averaged OCT image  $\bar{I}(x, z)$  and contains the average signal intensity from 100 consecutive images. The red image is a motility map  $M(x, z)$  displaying the motility amplitude at each pixel, calculated from the same 100 images. The two continuous lines at the bottom of each image correspond to the top and bottom surfaces of the PET film. The blue features above the film correspond to paper fibers of the scaffolds as well as time-averaged signals from the cells themselves. Figure 2(c) and (d) contain solid yellow lines to identify the top and bottom boundaries of the invasion assay and dashed yellow lines to identify the interfaces between the four layers of the cell-laden and cell-free cultures. Paper fibers are a highly scattering static structure, with high signal intensity but low fluctuation, resulting in low  $M$  values. Regions with live cells exhibiting intracellular motion resulted in large  $M$  values. By superimposing a red motility map onto the blue OCT image, the operator detected the positions of the live cells and correctly distinguished the cell-laden and cell-free cultures. These differences in motility between the cell-laden and cell-free assays are also visible in their corresponding time-lapse videos, as shown in Visualization 1. Motility observed in regions outside the scaffolds was attributed to Brownian motions of wax that detached from the paper scaffolds.

#### 3.2. Validation of OCT motility analysis by comparison with fluorescence imaging

To validate that OCT could accurately quantify the distribution of cells throughout a three-day invasion assay, we compared the OCT determined  $P_{Li}$  values with those determined from fluorescence images. To account for the time-dependent nature of cellular movement, we prepared four invasion cultures on Day 0 using the same passage of cells. On each day, a single culture was imaged by OCT to obtain a 4D (3D in space and 1D in time for motility) set of OCT data (see Visualization 2 for a representative lateral fly-through in space of a single assay analyzed on Day 3), and then immediately destacked and analyzed with fluorescence imaging. The Day 0

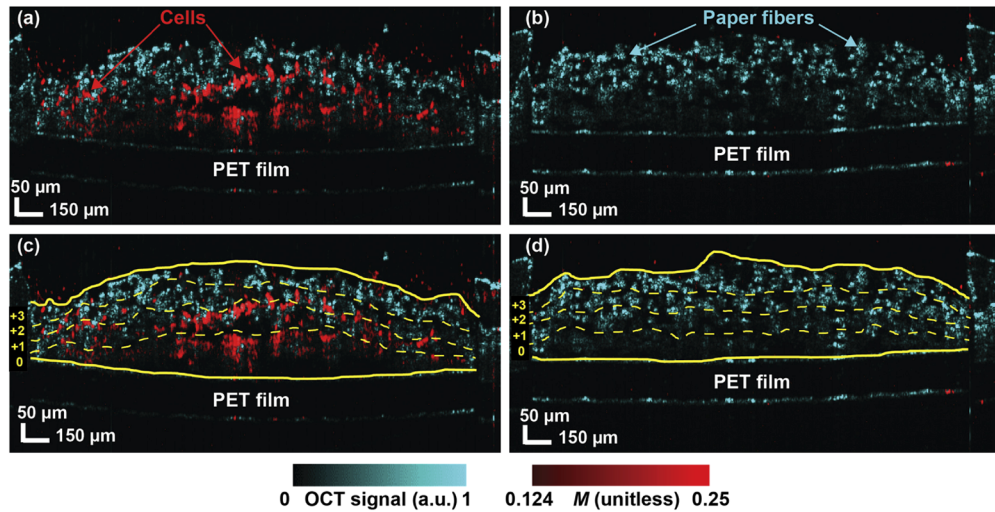


**Fig. 2.** Representative motility-contrasted OCT images of a 4-layer (a) cell-laden and (b) cell-free invasion assay. Both cultures were imaged after 3 days of incubation. Each image is a superposition of a motility map  $M(x, z)$  (red) with the time-averaged OCT image  $\bar{I}(x, z)$  (blue). Representative manual segmentation lines depicting the four layers of the (c) cell-laden and (d) cell free invasion assays. The solid yellow lines represent the top and bottom boundaries of the invasion assay; the three yellow dashed lines represent the interfaces between the four scaffolds of the assay. The time-averaged OCT images reveal static components of culture structures, while the motility map is specific to dynamic components, predominantly from live cells. Corresponding time-lapse videos through each OCT stack reveal the speckle fluctuations that cause the motility map of the cell-laden culture (see [Visualization 1](#)). To improve the visibility of the cells, these images were mean filtered by the size of a cell ( $9 \mu\text{m} \times 9 \mu\text{m}$ ) and a corresponding threshold,  $M > 0.124$ , was applied to  $M$  at every pixel to reject background noise.

culture was imaged approximately one hour after assembly and served as a baseline measure for a setup in which no invasion was expected to occur. The remaining cultures were analyzed approximately every 24 hours by both methods. OCT imaging took an average of 2 hours to collect the 4D data for 4 separate invasion assays within the culture; the fluorescence images were taken approximately one hour later. The use of a single sample for each day's analysis served two purposes. First, it minimized any biological or time-dependent variation that could result in different  $P_{Li}$  distributions. Second, it paired the analyses, which allowed us to compare the two imaging techniques directly.

Figure 3 contains plots of the  $P_{Li}$  distributions determined by both OCT motility analysis and fluorescence imaging on Days 0–3. On Day 0, both analysis techniques showed that approximately 80% of the cells remained in layer 0. By Day 1, 15–40% of the cells invaded layer +1. By Day 2, 40–50% of cells invaded layer +1 and approximately 10% of the cells invaded layer +2. By Day 3, fewer than 40% of the cells remained in layer 0 and up to 17% of the cells reached layer +3, invading at least  $120 \mu\text{m}$  ( $\sim 40 \mu\text{m}/\text{scaffold}$ ). These values are experimentally reasonable and match distributions obtained with MDA-MB-231 cells in PBCs previously [10,12]. Direct comparisons with other setups are difficult, as the extent of invasion is dependent upon factors such as assay duration, ECM composition, and the presence of extracellular gradients [41]. For example, others showed that 15–80% of MDA-MB-231 cells invaded across ECM-modified Transwells or through an in ECM gel slab in less than 72h [42,43].

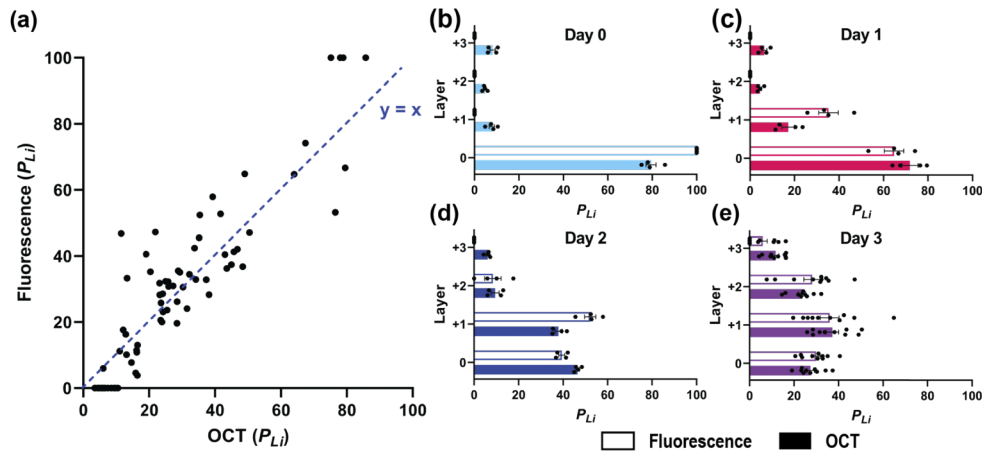


**Fig. 3.** Four invasion cultures were prepared from a single cell passage, then, one culture was selected on each day for analysis by OCT immediately followed by fluorescence imaging. (a) Scatter plot comparing the OCT and fluorescence imaging  $P_{Li}$  values from 22 separate invasion assays ( $n = 88$ ). A 45-degree dashed line is included to indicate the similarity between the two methods and the calculated ICC value of 0.903 (95% confidence interval, 0.867–0.941) indicates that the two methods are highly correlated. (b – e) End-point  $P_{Li}$  distributions determined with OCT and from fluorescence images after approximately (b) zero, (c) one, (d) two, and (e) three days of incubation. Each bar represents the average and SEM of cells in each layer of the invasion assay from a minimum of  $n = 4$  technical replicates. Individual data points are shown as black dots. Each bar also represents the minimum distance the cells must have invaded to reach the next layer, as each scaffold is 40–75  $\mu\text{m}$  thick.

To compare the abilities of OCT and fluorescence imaging to convert the detected signal into the percentage of viable cells distributed throughout the invasion assay (*i.e.*, the  $P_{Li}$  values), we estimated the ICC for 22 separate invasion assays. Figure 3(a) includes all paired  $P_{Li}$  values from four separate invasion cultures analyzed over a three-day period. Each data point is paired because both imaging techniques were used to analyze the same invasion assay. Both the 45-degree line placed on the scatterplot and the ICC of 0.903 (95% confidence interval, 0.867–0.941) show the two methods are highly correlated and that OCT is capable of measuring cellular viability.

Figures 3(b–e) are the cell distributions determined by both methods on Days 0–3. To determine if the cell distributions from each day were equivalent, given the normality of the difference held for each orthogonal transformed variable, we used a paired  $t$ -test to compare each of three orthogonally transformed variables between the two groups, and applied the Holm-Bonferroni sequentially rejective test procedure to adjust the  $p$ -values. Table 1 shows the adjusted step-down  $p$ -values for Figs. 3(b–e) and Fig. 4(a). As shown in Table 1, at least one of the three adjusted step-down  $p$ -values for Days 0 and 2 were smaller than the pre-specified significance level (0.05), indicating there was a significant difference between the cell distributions determined by OCT and fluorescence imaging. All the adjusted step-down  $p$ -values for both Days 1 and 3 were larger than the pre-specified significance level of 0.05, indicating there was no statistically significant difference in the cell distributions.

One possible reason for the differences in cell distributions between the two techniques was the manner in which LOD thresholds were applied. The fluorescence imaging resolution (200  $\mu\text{m}$ ) was unable to distinguish individual MDA-MB-231 cells ( $\sim 12 \mu\text{m}$  in diameter), requiring average fluorescence intensity be taken over the entire zone. The LOD was calculated similarly, taking the average fluorescence intensity of entire cell-free zones. By this method, the calculated LOD

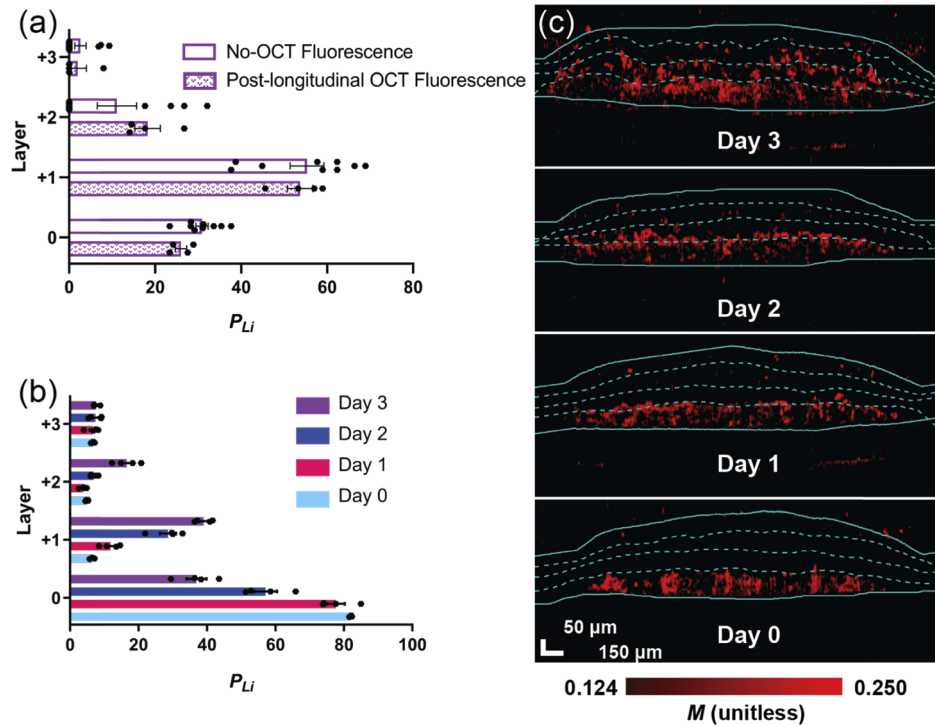


**Fig. 4.** (a)  $P_{LI}$  distributions of two separate invasion cultures determined with fluorescence imaging, after a three-day incubation. The post-longitudinal OCT fluorescence values correspond to an end-point measure of an invasion culture whose cell distributions were analyzed with OCT on Days 0–3. The no-OCT fluorescence values correspond to an end-point measure of an invasion culture that was not exposed to OCT. (b)  $P_{LI}$  distributions measured with OCT for Days 0–3. (c) Representative OCT motility images for Days 0–3; blue lines show the manually segmented scaffolds (bottom to top: scaffold 0–3). To improve the visibility of cells, these representative images were mean filtered by the size of a cell ( $9\ \mu\text{m} \times 9\ \mu\text{m}$ ) and a corresponding threshold,  $M > 0.124$ , was applied to  $M$  at every pixel to reject background noise. All bars are the average and SEM from a minimum of  $n = 4$  replicates. Each bar also represents the minimum distance the cells must have invaded to reach the next layer, as each scaffold is  $40\ \mu\text{m}$  thick.

**Table 1.** Holm-Bonferroni statistical test procedure adjusted step-down p-value results

| Samples      | Adjusted step-down p-value ( $V_1, V_2, V_3$ ) <sup>a</sup> |
|--------------|---|
| Fig. 3 Day 0 | (0.010, 0.010, 0.010)                                       |
| Fig. 3 Day 1 | (0.278, 0.278, 0.259)                                       |
| Fig. 3 Day 2 | (0.326, 0.004, 0.062)                                       |
| Fig. 3 Day 3 | (0.372, 0.372, 0.372)                                       |
| Fig. 4(a)    | (0.708, 0.365, 0.708)                                       |

<sup>a</sup>Null hypothesis was  $H_{i0} : \bar{\mu}_{1i} = \bar{\mu}_{2i}$ . p-values  $> 0.05$  indicated an acceptance of the null hypothesis and that the cell distributions of the two groups were statistically equivalent.

corresponded to  $\sim 5000$  cells. In comparison, the OCT image resolution corresponds to the size of a single cell. Thus, the LOD in OCT was applied on a pixel-by-pixel basis, retaining spatial heterogeneity of  $M$  during thresholding. This may have resulted in fewer cells being falsely thresholded to a value of zero than in the fluorescence images and a subsequently lower detection limit, which resulted in higher  $N_{Li}$  being detected in layers +2 and +3. Another possible reason for the differences between the two techniques was that OCT images were collected *in situ* and each layer was identified with manual segmentation, while fluorescence images were collected after destacking the culture forcing cells into a defined layer. As can be seen in Fig. 4(c) the manual segmentation lines intersected highly populated cell regions, which could have led to differences in  $P_{Li}$  distributions.

### 3.3. OCT does not significantly disturb cells in PBCs

Longitudinal measurements of a single sample are desirable because they decrease the biological and technical variability of the dataset. However, continued exposure of the focused,  $\sim 6$  mW, near-infrared laser beam needed for OCT measurements has the potential to damage the cells. To determine if repeat OCT measurements altered the extent of cellular invasion, we compared invasion cultures prepared on the same day, where one culture underwent repeated OCT imaging every day for three days (culture A) and the other was only imaged by fluorescence imaging on Day 3 (culture B). The longitudinal OCT imaging of culture A for Day 0 was performed  $\sim 1$  hour after assembly. Approximately 1 hour after the Day 3 OCT measurement of culture A, both cultures were disassembled and analyzed by fluorescence imaging. To determine if the cell distributions from cultures A and B were equivalent, given that the normality of the difference didn't hold for some orthogonal transformed variables in one group, we used a Wilcoxon rank sum test to compare each of the three orthogonally transformed variables between the two groups, and applied the Holm-Bonferroni sequentially rejective test procedure to adjust the  $p$ -values. As shown in Table 1, the adjusted step-down  $p$ -values, for Fig. 4(a), were all larger than the pre-specified significance level of (0.05), indicating that repeated exposure to the focused near-infrared laser beam did not result in statistically significant differences in the cell distribution.

### 3.4. Tracking cell invasion from Day 0 to Day 3 by longitudinal OCT motility analysis

Figure 4(b) plots the  $P_{Li}$  distributions collected as part of the longitudinal OCT experiment discussed above, using OCT to quantify changes in  $P_{Li}$  in a single PBC with increasing periods of incubation. Figure 4(c) contains representative motility-contrasted OCT images collected each day. Representative 3D visualization of invasion cultures on Day 0 and Day 3 by OCT are shown in Fig. 5. Corresponding 3D rendering of the OCT motility images at Day 0 and Day 3 for representative stacks are shown in Visualization 3. As expected from the end-point measurements in Fig. 3, we observed increased cellular invasion with increased incubation time. An advantage of longitudinal measurements is the ability to track variations due to differences in setting up each replicate invasion assay. For example, in layer 0 of Fig. 4(b) there is a single point that is visibly above the average signal across Days 1–3. In end-point analyses like those displayed in Fig. 3, it is not possible to identify anomalous points to the single measurements of many samples.

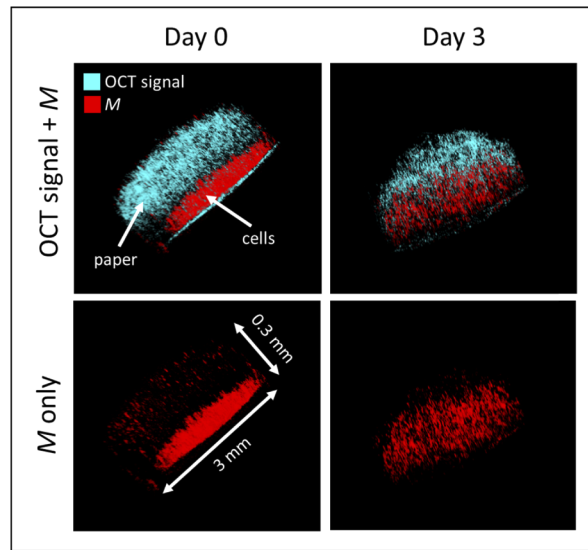


**Fig. 5.** Representative 3D visualization of invasion cultures on Day 0 and Day 3 by OCT (See Visualization 3). The top row shows OCT signals (blue) overlaid with motility amplitudes,  $M$  (red). The bottom row shows  $M$  alone. To improve the visibility of cells, these representative images were mean filtered by the size of a cell ( $9\ \mu\text{m} \times 9\ \mu\text{m}$ ) and a corresponding threshold,  $M > 0.124$ , was applied to  $M$  at every pixel to reject background noise.

#### 4. Conclusion

In this work, we demonstrate the ability of OCT to track the invasion of triple-negative breast cancer cells in 3D PBCs *in situ* and longitudinally. The ability to perform *in situ* measurements is a powerful advantage over fluorescence imaging, which requires the invasion culture to be disassembled prior to analysis. With OCT, experimental logistics are simplified as longitudinal studies eliminate sample-to-sample variability within datasets. Our results show that OCT can successfully differentiate cells from the fibers of the paper scaffold in a four-layer invasion stack. The  $\sim 4$  dB attenuation of the OCT signal between the top and bottom layers of the invasion stack suggest that even thicker structures would be amenable to these methods, depending on the SNR of the OCT system. Our previous work on OCT-based imaging of organoids supports this conclusion [28,31–32]. The measured  $P_{Li}$  values from OCT and fluorescence imaging are highly correlated. Evidence suggests that OCT also offers an additional advantage of a lower limit of detection. Longitudinal OCT measurements are capable of quantitatively tracking cellular invasion over 3 days, and potentially longer. As a non-destructive technique, OCT enables *in situ* invasion tracking to be paired with molecular analyses at the transcript and protein level on distinct subpopulations of cells that moved different distances.

#### Funding

National Cancer Institute (CA172904); National Institute of Environmental Health Sciences (P30ES010126); National Institute of General Medical Sciences (R35GM128697); Division of Chemical, Bioengineering, Environmental, and Transport Systems (1351473, 1803830).

#### Acknowledgments

We thank Prof. Gary Koch for helpful discussions and suggestions on computing the intraclass correlation coefficient between the datasets obtained with OCT and fluorescence imaging.

## Disclosures

The authors declare no conflicts of interest.

## References

1. C. L. Chaffer and W. A. Robert, "A perspective on cancer cell metastasis," *Science* **331**(6024), 1559–1564 (2011).
2. S. Breslin and L. O'Driscoll, "Three-dimensional cell culture the missing link in drug discovery," *Drug Discovery Today* **18**(5-6), 240–249 (2013).
3. B. Weigelt, C. M. Ghajar, and M. J. Bissell, "The need for complex 3D culture models to unravel novel pathways and identify accurate biomarkers in breast cancer," *Adv. Drug Delivery Rev.* **69-70**, 42–51 (2014).
4. K. M. Yamada and E. Cukierman, "Modeling tissue morphogenesis and cancer in 3D," *Cell* **130**(4), 601–610 (2007).
5. P. Friedl and S. Alexander, "Cancer invasion and the microenvironment: plasticity and reciprocity," *Cell* **147**(5), 992–1009 (2011).
6. V. Brekhman and G. Neufeld, "An asymmetric 3D In vitro assay for the study of tumor cell invasion," *Methods Cell Biol.* **112**, 311–328 (2012).
7. A. Albin, Y. Iwamoto, and H. K. Kleinman, "A rapid in vitro assay for quantitating the invasive potential of tumor cells," *Cancer Res.* **47**, 3239–3245 (1987).
8. M. H. Zaman, L. M. Trapani, A. L. Sieminski, D. Mackellar, H. Gong, R. D. Kamm, A. Wells, D. A. Lauffenburger, and P. Matsudaira, "Migration of tumor cell in 3D matrices is governed by matrix stiffness along with cell-matrix adhesion and proteolysis," *Proc. Natl. Acad. Sci.* **103**(29), 10889–10894 (2006).
9. E. Wiercinska, H. P. H. Naber, E. Pardali, G. Van Der Pluijm, H. Van Dam, and P. Ten Dijke, "The TGF- $\beta$ /Smad pathway induces breast cancer cell invasion through the up-regulation of matrix metalloproteinase 2 and 9 in a spheroid invasion model system," *Breast Cancer Res. Treat.* **128**(3), 657–666 (2011).
10. R. M. Kenney, M. W. Boyce, A. S. Truong, C. R. Bagnell, and M. R. Lockett, "Real-time imaging of cancer cell chemotaxis in paper-based scaffolds," *Analyst* **141**(2), 661–668 (2016).
11. R. M. Kenney, A. Loeser, N. A. Whitman, and M. R. Lockett, "Paper-based transwell assays: an inexpensive alternative to study cellular invasion," *Analyst* **144**(1), 206–211 (2019).
12. A. S. Truong, C. A. Lochbaum, M. W. Boyce, and M. R. Lockett, "Tracking the invasion of small numbers of cells in paper-based assays with quantitative PCR," *Anal. Chem.* **87**(22), 11263–11270 (2015).
13. C. C. Lloyd, M. W. Boyce, and M. R. Lockett, "Paper-based invasion assays for quantifying cellular movement in three-dimensional tissue-like structures," *Curr. Protoc. Chem. Biol.* **9**(2), 75–95 (2017).
14. B. Mosadegh, B. E. Dabiri, M. R. Lockett, R. Derda, P. Campbell, K. K. Parker, and G. M. Whitesides, "Three-dimensional paper-based model for cardiac ischemia," *Adv. Healthcare Mater.* **3**(7), 1036–1043 (2014).
15. G. Camci-Unal, D. Newsome, B. K. Eustace, and G. M. Whitesides, "Fibroblasts enhance migration of human lung cancer cells in a paper-based coculture system," *Adv. Healthcare Mater.* **5**(6), 641–647 (2016).
16. B. Mosadegh, M. R. Lockett, K. T. Minn, K. A. Simon, K. Gilbert, S. Hillier, D. Newsome, H. Li, A. B. Hall, D. M. Boucher, B. K. Eustace, and G. M. Whitesides, "A paper-based invasion assay: assessing chemotaxis of cancer cells in gradients of oxygen," *Biomaterials* **52**, 262–271 (2015).
17. M. W. Boyce, G. J. Labonia, A. B. Hummon, and M. R. Lockett, "Assessing chemotherapeutic effectiveness using a paper-based tumor model," *Analyst* **142**(15), 2819–2827 (2017).
18. D. Huang, E. A. Swanson, C. P. Lin, J. S. Schuman, W. G. Stinson, W. Chang, M. R. Hee, T. Flotte, K. Gregory, C. A. Puliafito, J. G. Fujimoto, C. P. Lin, J. S. Schuman, and C. A. Puliafito, "Optical Coherence Tomography," *Science* **254**, 1178–1181 (1991).
19. A. F. Fercher, W. Drexler, C. K. Hitzenberger, and T. Lasser, "Optical coherence tomography - principles and applications," *Rep. Prog. Phys.* **66**(2), 239–303 (2003).
20. P. Yu, M. Mustata, J. J. Turek, P. M. W. French, M. R. Melloch, and D. D. Nolte, "Holographic optical coherence imaging of tumor spheroids," *Appl. Phys. Lett.* **83**(3), 575–577 (2003).
21. R. K. Chhetri, Z. F. Phillips, M. A. Troester, and A. L. Oldenburg, "Longitudinal study of mammary epithelial and fibroblast co-cultures using optical coherence tomography reveals morphological hallmarks of pre-malignancy," *PLoS One* **7**(11), e49148 (2012).
22. S. A. Boppart, W. Tan, H. J. Ko, and C. Vinegoni, "Optical coherence tomography of cell dynamics in three-dimensional engineered tissues," *Optical Coherence Tomography and Coherence Techniques II* (Optical Society of America, 2005).
23. S. M. Rey, B. Považay, B. Hofer, A. Unterhuber, B. Hermann, A. Harwood, and W. Drexler, "Three- and four-dimensional visualization of cell migration using optical coherence tomography," *J. Biophotonics* **2**(6-7), 370–379 (2009).
24. K. K. Chu, M. E. Kusek, L. Liu, A. Som, L. M. Yonker, H. Leung, D. Cui, J. Ryu, A. D. Eaton, G. J. Tearney, and B. P. Hurley, "Illuminating dynamic neutrophil trans-epithelial migration with micro-optical coherence tomography," *Sci. Rep.* **8**, 45789 (2017).
25. P. Yu, L. Peng, M. Mustata, J. J. Turek, M. R. Melloch, and D. D. Nolte, "Time-dependent speckle in holographic optical coherence imaging and the health of tumor tissue," *Opt. Lett.* **29**(1), 68–70 (2004).
26. Z. Li, H. Sun, J. Turek, S. Jalal, M. Childress, and D. D. Nolte, "Doppler fluctuation spectroscopy of intracellular dynamics in living tissue," *J. Opt. Soc. Am. A* **36**(4), 665 (2019).

27. K. Jeong, J. J. Turek, and D. D. Nolte, "Speckle fluctuation spectroscopy of intracellular motion in living tissue using coherence-domain digital holography," *J. Biomed. Opt.* **15**(3), 030514 (2010).
28. X. Yu, A. M. Fuller, R. Blackmon, M. A. Troester, and A. L. Oldenburg, "Quantification of the effect of toxicants on the intracellular kinetic energy and cross-sectional area of mammary epithelial organoids by OCT fluctuation spectroscopy," *Toxicol. Sci.* **162**(1), 234–240 (2018).
29. A. L. Oldenburg, R. K. Chhetri, J. M. Cooper, W.-C. Wu, M. A. Troester, and J. B. Tracy, "Motility-, autocorrelation-, and polarization-sensitive optical coherence tomography discriminates cells and gold nanorods within 3D tissue cultures," *Opt. Lett.* **38**(15), 2923 (2013).
30. C. Apelian, F. Harms, O. Thouvenin, and A. C. Boccara, "Dynamic full field optical coherence tomography: subcellular metabolic contrast revealed in tissues by interferometric signals temporal analysis," *Biomed. Opt. Express* **7**(4), 1511 (2016).
31. A. L. Oldenburg, X. Yu, T. Gilliss, O. Alabi, R. M. Taylor, and M. A. Troester, "Inverse-power-law behavior of cellular motility reveals stromal–epithelial cell interactions in 3D co-culture by OCT fluctuation spectroscopy," *Optica* **2**(10), 877 (2015).
32. L. Yang, X. Yu, A. M. Fuller, M. A. Troester, and A. L. Oldenburg, "Characterizing optical coherence tomography speckle fluctuation spectra of mammary organoids during suppression of intracellular motility," *Quant. Imaging Med. Surg.* **10**(1), 76–85 (2020).
33. K. B. Yin, "The Mesenchymal-like Phenotype of the MDA-MB-231 Cell Line," *Breast Cancer* (IntechOpen, 2012), Chapter 18.
34. J. Schindelin, I. Arganda-Carreras, E. Frise, V. Kaynig, M. Longair, T. Pietzsch, S. Preibisch, C. Rueden, S. Saalfeld, B. Schmid, J.-Y. Tinevez, D. J. White, V. Hartenstein, K. Eliceiri, P. Tomancak, and A. Cardona, "Fiji: an open-source platform for biological-image analysis," *Nat. Methods* **9**(7), 676–682 (2012).
35. G. L. Long and J. D. Winefordner, "Limit of detection: a closer look at the IUPAC definition," *Anal. Chem.* **55**(7), 712A–724A (1983).
36. R. K. Chhetri, K. A. Kozek, A. C. Johnston-Peck, J. B. Tracy, and A. L. Oldenburg, "Imaging three-dimensional rotational diffusion of plasmon resonant gold nanorods using polarization-sensitive optical coherence tomography," *Phys. Rev. E* **83**(4), 040903 (2011).
37. D. L. Marks, A. L. Oldenburg, J. J. Reynolds, and S. a Boppart, "Digital algorithm for dispersion correction in optical coherence tomography for homogeneous and stratified media," *Appl. Opt.* **42**(2), 204–217 (2003).
38. J. L. Fleiss, *The Design and Analysis of Clinical Experiments* (John Wiley & Sons, Inc., 1999).
39. G. G. Koch, "Intraclass correlation coefficient," *Encycl. Stat. Sci.* 212–217 (1982).
40. S. Holm, "A simple sequential rejective method procedure," *Scand. J. Stat.* **6**, 65–70 (1979).
41. J. Sapudom, S. Rubner, S. Martin, T. Kurth, S. Riedel, C. T. Mierke, and T. Pompe, "The phenotype of cancer cell invasion controlled by fibril diameter and pore size of 3D collagen networks," *Biomaterials* **52**, 367–375 (2015).
42. P. J. Magee, H. McGlynn, and I. R. Rowland, "Differential effects of isoflavones and lignans on invasiveness of MDA-MB-231 breast cancer cells in vitro," *Cancer Lett.* **208**(1), 35–41 (2004).
43. R. Poincloux, O. Collin, F. Lizárraga, M. Romao, M. Debray, M. Piel, and P. Chavrier, "Contractility of the cell rear drives invasion of breast tumor cells in 3D Matrigel," *Proc. Natl. Acad. Sci.* **108**(5), 1943–1948 (2011).